THE JOURNAL OF BIOLOGICAL CHEMISTRY VOL. 284, NO. 37, pp. 25404–25411, September 11, 2009

An Oligomeric Signaling Platform Formed by the Toll-like Receptor Signal Transducers MyD88 and IRAK-4*[S]

Received for publication, May 18, 2009, and in revised form, June 23, 2009 Published, JBC Papers in Press, July 10, 2009, DOI 10.1074/jbc.M109.022392

Precious G. Motshwene[‡1], Martin C. Moncrieffe[‡2], J. Günter Grossmann[§], Cheng Kao[¶], Murali Ayaluru[¶], Alan M. Sandercock[‖], Carol V. Robinson[‖], Eicke Latz[**], and Nicholas J. Gay[‡3]

*From the [‡]Department of Biochemistry, University of Cambridge, Cambridge CB2 1GA, United Kingdom, the [§]Molecular Biophysics Group, School of Biological Sciences, University of Liverpool, Liverpool L69 7ZB, United Kingdom, the [‖]Department of Chemistry, University of Cambridge, Cambridge CB2 1EW, United Kingdom, the [¶]Department of Biochemistry and Biophysics, Texas A&M University, College Station, Texas 77843, and the **Department of Medicine, Division of Infectious Disease, University of Massachusetts Medical School, Worcester, Massachusetts 01655*

Toll-like receptors (TLRs) mediate responses to pathogen-associated molecules as part of the vertebrate innate immune response to infection. Receptor dimerization is coupled to downstream signal transduction by the recruitment of a post-receptor complex containing the adaptor protein MyD88 and the IRAK protein kinases. In this work, we show that the death domains of human MyD88 and IRAK-4 assemble into closed complexes having unusual stoichiometries of 7:4 and 8:4, the Myddosome. Formation of the Myddosome is likely to be a key event for TLR4 signaling *in vivo* as we show here that pathway activation requires that the receptors cluster into lipid rafts. Taken together, these findings indicate that TLR activation causes the formation of a highly oligomeric signaling platform analogous to the death-inducing signaling complex of the Fas receptor pathway.

In vertebrates, the initial responses of innate immunity are mediated by a family of pattern recognition receptors, which are able to sense the presence of a variety of microbial products such as lipids and non-self nucleic acid (1). One important family of pattern recognition receptors is the Toll-like receptors (TLRs)[4] that are expressed by many immune system cell types such as macrophages and dendritic cells. TLRs are class one transmembrane receptors that are activated by a process of stimulus-induced dimerization of their extracellular domains. This in turn causes the cytoplasmic Toll/interleukin-1 (IL-1) domains (TIRs) to dimerize, forming a scaffold for the recruitment of downstream signaling components (2). TLRs use five signaling adaptor proteins to couple receptor activation to downstream signal transduction (3). All of these adaptors have TIRs and engage with the activated TLRs by TIR-TIR interactions.

One of the adaptor proteins, MyD88, is of particular importance because it is used by all but one of the TLRs as well as by the IL-1 and interferon-γ receptors. MyD88-deficient mice have profoundly impaired innate immune responses and are susceptible to a wide range of infectious diseases. The MyD88 sequence is tripartite and is comprised of a death domain (DD) at the N terminus, a short (40-amino-acid) intermediate domain (ID) of unknown structure, and a C-terminal TIR. Evidence from yeast two-hybrid experiments suggests that MyD88 can self-associate with contacts in both the DD and the TIR (4). The current view of post-receptor signal transduction is that two MyD88 TIR domains bind to the activated TLR, and this enables the recruitment of the protein kinases IRAK-4 and IRAK-1 (5). These kinases have DDs at their N termini, and both are recruited into a complex with MyD88 after signal initiation. It appears that IRAK-4 is recruited first, and this binding requires the ID of MyD88 (6, 7). Thus MyD88s, a splice variant that lacks the ID, down-regulates TLR signaling and cannot recruit IRAK-4 into the post-receptor complex. In contrast, IRAK-1 interacts with MyD88s presumably by DD-DD rather than DD-ID interactions. The next step in the signaling process is for IRAK-4 to phosphorylate IRAK-1, causing activation of the latter and hyper-autophosphorylation. IRAK-1 then dissociates from the complex and interacts with the ubiquitin-protein isopeptide ligase (E3) TRAF6 (8, 9).

DDs together with the structurally related caspase recruitment domains (CARDs) and death effector domains (DEDs) form the death domain superfamily (10). There are 215 proteins encoded by the human genome that are predicted to have this fold, and they are widely used in cellular signaling including the TLR and apoptotic pathways. Structurally, DDs contain six antiparallel α-helices, and they are predominantly involved in protein-protein interactions with other DDs. Three modes of DD-DD interaction, types 1, 2, and 3 (10), have been characterized and are illustrated by the structures of the *Drosophila*

* This work was supported in part by grants from the UK Medical Research Council and Biotechnology and Biological Science Research Council (to N. G.).
[S] The on-line version of this article (available at http://www.jbc.org) contains supplemental Figs. S1 and S2.
[1] Supported by the South African National Research Foundation.
[2] To whom correspondence may be addressed: Dept. of Biochemistry, University of Cambridge, 80 Tennis Court Road, Cambridge, CB2 1GA. Fax: 44-1-223-766002; E-mail: mcm35@cam.ac.uk.
[3] To whom correspondence may be addressed: Dept. of Biochemistry, University of Cambridge, 80 Tennis Court Road, Cambridge, CB2 1GA. Fax: 44-1-223-766002; E-mail: njg11@cam.ac.uk.
[4] The abbreviations used are: TLR, Toll-like receptor; TIR, Toll/IL-1 receptor domain; TRIF, TIR domain containing adaptor protein inducing interferon β; MyD88, myeloid differentiation factor 88; IRAK, interleukin 1 receptor-associated kinase; IL, interleukin; DD, death domain; ID, intermediate domain; BS3, bis(sulphosuccinimydyl) suberate; DISC, death-induced signaling complex; PIDD, p53-induced death domain protein; RAIDD, RIP-associated ICH-1/CED-3-homologous protein with a death domain; ELISA, enzyme-linked immunosorbent assay; AUC, analytical ultracentrifugation; SAXS, small angle x-ray scattering; FADD, Fas-associated death domain; LPS, lipopolysaccharide; HEK, human embryonic kidney; YFP, yellow fluorescent protein; h, human; d, *Drosophila*.

Tube-Pelle heterodimer (11), the Procaspase-9 homodimer (12), and most remarkably, by the PIDDosome (13). In the latter case, PIDD, RAIDD, and Caspase-2 form a complex, which results in the proximity-induced activation of Caspase-2 protease activity, which in turn leads to cytochrome *c* release and apoptotic cell death. The DDs of PIDD and RAIDD interact to produce a complex having a stoichiometry of 5:7, and the subunits are arranged in three layers with five PIDDs, five RAIDDs, and then two RAIDDs. The structure is stabilized by 25 DD-DD contacts of which six are type 2, nine are type 1, and 10 are type 3.

In this study, we report that like PIDD and RAIDD, the DDs of human MyD88 and IRAK-4 assemble into defined structures having stoichiometries of 7:4 and 8:4. We propose that the structure has two layers with a ring of seven or eight MyD88 subunits and a second layer of four IRAK-4 subunits. The formation of these higher order assemblies provides insight into the complex regulation and cross-talk observed in the TLR signaling pathways.

EXPERIMENTAL PROCEDURES

Sample Preparation—The death domains of both IRAK-4 and human MyD88 (hMyD88) were cloned into the pETG-30 (AGeerlof, European Molecular Biology Laboratory (EMBL)) expression vector and transformed into BL21 Codon Plus (Novagen) (IRAK-4 DD) and BL21-DE3 (Novagen) (hMyD88). Proteins were expressed in LB media with appropriate antibiotics. Cells containing IRAK-4 DD or hMyD88 DD were resuspended in 20 mM Tris, pH 8.0, and lysed. The lysate was centrifuged at 1050 × *g* for 1 h, and the supernatant was loaded onto glutathione-Sepharose column and eluted with 20 mM Tris with or without 50 mM NaCl, pH 8.0, 40 mM reduced glutathione. After cleavage of the glutathione *S*-transferase tag, the solution was loaded onto a nickel-nitrilotriacetic acid column to remove cleaved glutathione *S*-transferase. Protein solutions were concentrated, and the individual death domains were purified using ion-exchange followed by a Superdex 75 size exclusion column with the same buffer supplemented with 5 mM dithiothreitol. The hMyD88-IRAK-4 complex was prepared by adding a slight molar excess of IRAK-4 DD, and the complex was purified using a Superdex 200 column. Purity at all stages was assessed by SDS-PAGE.

Antibodies and Cell Culture—The HTA125 antibody was a gift from Dr. K. Miyake (University of Tokyo). The anti-CD14 antibody 26ic was purified from hybridoma cells (American Type Culture Collection (ATCC, Rockville, MD), and anti-TLR2 (TL2.1) was a gift from Terje Espevik (Norwegian University of Science and Technology (NTNU), Trondheim, Norway). Antibodies were immobilized on sterile high protein binding polystyrene 96-well plates (Corning) for 16 h in phosphate-buffered saline. After three washes with phosphate-buffered saline, 7×10^5 HEK293 cells were added in growth medium. After 18 h, supernatants were harvested, and concentrations of IL-8 were measured by ELISA. MD-2 was supplied in supernatants from MD-2-transfected HEK cells. Generation of stable HEK293-TLR4 cells has been described previously (14).

Chemical Cross-linking of Proteins—This was performed with bis(sulfosuccinimidyl) suberate BS3 using an established protocol (15).

Analytical Ultracentrifugation—Sedimentation velocity measurements were performed using a Beckman XL-A analytical ultracentrifuge equipped with absorbance and interference optics. Absorption data (280 nm) were acquired at 20 °C and a rotor speed of 60,000 rpm with an An60-Ti (Beckman Coulter) rotor. Partial specific volumes, buffer density, and viscosity were calculated using SEDNTERP, and the data were analyzed using the program SEDFIT (16).

Small Angle X-ray Scattering—X-ray scattering data of the hMyD88-IRAK-4 DD complex in solution were collected at 4 °C at the Synchrotron Radiation Source (Daresbury, UK) using sample-to-detector distances of 1 and 4.5 m and protein concentrations of 6.8–2.5 mg/ml. The scattering intensities at both detector distances and for each sample were merged, and the program GNOM (17) was used to calculate the radius of gyration (R_g) and the maximum molecular dimension (d_{max}) via the distance distribution function, P_r. The scattering profiles were then used in *ab initio* shape restorations using the program GASBOR (18). Fifty independent shape reconstructions were performed assuming no symmetry constraints. The resulting shapes were subsequently aligned, averaged, and filtered using the DAMAVER (19) and SUPCOMB (20) packages.

Mass Spectrometry—The hMyD88-IRAK-4 complex was buffer-exchanged into ammonium acetate solution (200 mM, pH 7), using Biospin 6 micro-spin columns (Bio-Rad Laboratories). Mass spectrometry of intact complexes was performed as described previously (21). Briefly, samples were ionized by nano-electrospray ionization using gold-coated glass capillaries, prepared in-house. Mass spectra were acquired in the positive ion mode on a Synapt-HDMS mass spectrometer (Waters) fitted with a 32-kDa quadrupole, using argon gas in the trap/transfer T-wave regions and nitrogen gas in the IMS T-wave cell. Ion activation and collision-induced dissociation were achieved by raising the collision energy in the trap T-wave region. Mass spectrometry data were calibrated using $Cs_nI_{n-1}^+$ clusters and were processed and analyzed using Masslynx.

Electron Microscopy—The MyD88-IRAK-4 complex of 10 ng/ml in 20 mM Tris (pH 7.5) buffer was stained with 1% uranyl acetate on a freshly glow-discharged 400 mesh carbon-coated copper grid (Electron Microscopy Sciences, Hatfield, PA, catalog number CF400-Cu). The grids were viewed at a JEOL 1200 EX TEM, operated at 100 kV and at a calibrated magnification of 39,000. The micrographs were scanned on an Epson projection 3200 scanner at 1200 dpi corresponding to 5.5 Å/pixels at the specimen level.

Three-dimensional reconstructions was carried out using EMAN (version 1.8) (22) following the procedure described by Murali *et al.* (23). More than 10,000 particles were selected using the *boxer* routine from EMAN, and they were aligned and centered using the *cenalignint* routine from EMAN. Class averages were generated using *refine2d*. An initial model was generated from the representative noise-free class averages and used as a starting model. As the class averages appeared to be heterogeneous, we subjected the entire particle data set to

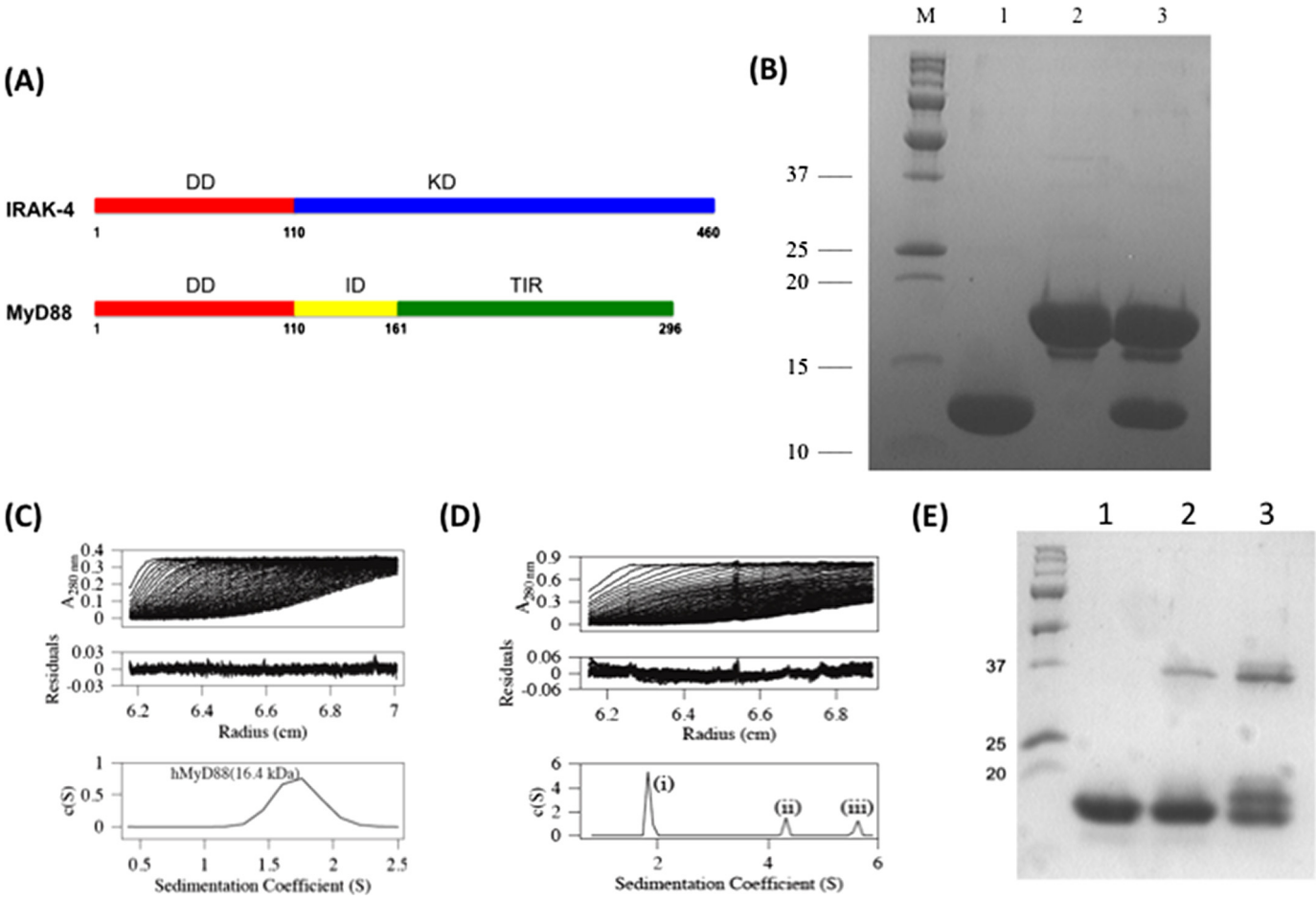

FIGURE 1. **Solution properties of the MyD88 and IRAK-4 death.** *A*, schematic representation of hMyD88 and IRAK-4 showing the DD, the ID, the TIR, and the kinase domain (*KD*). *B*, SDS-PAGE of purified proteins: IRAK-4 DD-(1–110) (*lane 1*); hMyD88 DD-ID-(1–152) (*lane 2*), and the hMyD88-IRAK-4 complex (*lane 3*). *M*, molecular mass marker. *C*, sedimentation velocity AUC profiles and the *c(S)* distributions for hMyD88 death domains (at 4 and 0.3 mg ml^{-1}). *D*, sedimentation velocity AUC profiles and the *c(S)* distributions for hMyd88 at 0.8 mg ml^{-1}. When compared with *C*, additional peaks are present representing oligomers of 100 and 150 kDa. *E*, chemical cross-linking of MyD88 protein (see "Experimental Procedures"). *Lane 1*, no treatment; *lane 2*, 0.02 mM bis(sulfosuccinimidyl) suberate; *lane 3*, 0.2 mM bis(sulfosuccinimidyl) suberate.

multi-refinement with three models. Two of the models were converged well as evidenced by the Fourier shell correlation and by the similarity between the class averages and projections of the model. The models were normalized to a molecular mass of 170 kDa and visualized using the University of California, San Francisco (UCSF) Chimera software (24).

RESULTS

Reversible Self-association of the MyD88 Death Domain—To study the interactions between hMyD88 and IRAK-4, we expressed sequences corresponding to the hMyD88 death and intermediate domains (amino acids 1–152) and the IRAK-4 death domain (amino acids 1–117) (see "Experimental Procedures" and Fig. 1, *A* and *B*). The protein preparations were then purified by ion-exchange and size exclusion chromatography. IRAK-4 DD elutes from gel filtration columns at a position that is consistent with the protein being a monomer irrespective of the ionic strength, and this conclusion is confirmed by analytical ultracentrifugation (AUC) (Fig. 1*C*). In contrast, the oligomeric state of hMyD88 depends on both concentration and ionic strength. At concentrations less than 0.4 mg/ml, hMyD88 exists as monomer (Fig. 1*C*), but at higher concentrations oligomers of 100 and 150 kDa can be detected (Fig. 1*D*). The association is reversible, and dilution to concentrations of 0.3–0.4 mg/ml results in reformation of monomeric hMyD88. The tendency of hMyD88 to self-associate is significantly reduced with the addition of 50 mM NaCl and 5 mM dithiothreitol, and under these solution conditions, the protein is essentially monomeric (Fig. 1*C*). We then carried out chemical cross-linking experiments using BS3, a bifunctional reagent that reacts with lysine side chains. BS3 caused the formation of covalently cross-linked dimers, but no higher oligomers were detected even at high concentrations of cross-linker (Fig. 1*E*).

Taken together, these results show that MyD88 has an intrinsic propensity to oligomerize and that there are at least two modes of binding between MyD88 subunits. The oligomerization of MyD88 DD is also reversible, indicating that these homotypic interactions are of low affinity.

hMyD88 and IRAK-4 Death Domains Assemble into Stable Complexes with Stoichiometries of 7:4 and 8:4—The MyD88 DD preparation shown in Fig. 1*C* was mixed with a slight molar excess of IRAK-4 DD, and the products were separated on a calibrated gel filtration column. As shown in Fig. 2*A*, the MyD88-IRAK-4 complex elutes as a single peak within the

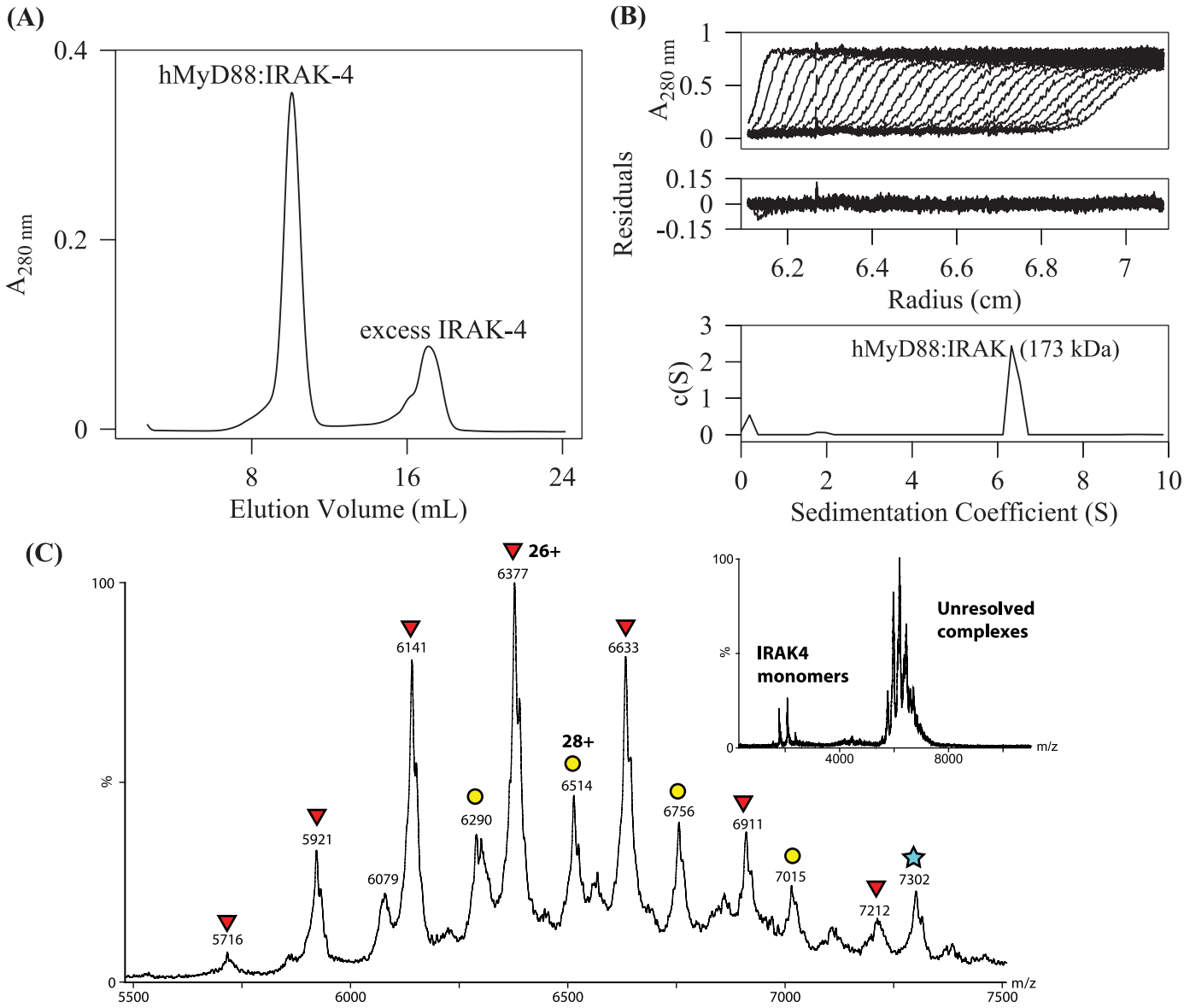

FIGURE 2. **hMyD88 and IRAK-4 death domains assemble into complexes with stoichiometries of 7:4 and 8:4.** *A*, elution profile of the hMyD88-IRAK-4 complex on a Superdex S200 gel filtration column. hMyD88 and IRAK-4 death domains were mixed to give a slight molar excess of IRAK-4. Samples from peak 1 and peak 2 are shown in Fig. 1*B*, *lanes 3* and *1*, respectively. Calibration of the column gave molecular mass estimates of 175 kDa for peak 1 and 12 kDa for peak 2 (not shown). *B*, sedimentation velocity data and the *c(S)* distribution for the hMyD88-IRAK-4 DD complex. *C*, nano-electrospray ionization mass spectra of MyD88-IRAK-4 complexes acquired under conditions that preserve non-covalent interactions. *Inset*, mass spectrum acquired with minimal gas phase activation, showing IRAK-4 monomers at low *m/z* and a set of poorly resolved ion series at higher *m/z*. *Main panel*, mass spectra acquired with moderate gas phase collisional activation to remove solvent adducts. Two well resolved overlapping ion series are revealed, corresponding to complexes with MyD88-IRAK-4 stoichiometries of 7:4 (*red triangles*, observed mass = 165,800 ± 34 Da, expected mass = 165,725 Da) and 8:4 (*yellow circles*, observed mass = 182,372 ± 6 Da, expected mass = 182,284 Da). Further unresolved ions are evident in the noise. (The *starred peak* forms part of an ion series extending to higher *m/z*, arising from gas phase dissociation of complexes; see supplemental Fig. 1.)

inclusion volume of the column, but surprisingly with an estimated molecular mass of 175 kDa, suggesting that a higher order complex had formed (see also Fig. 1*B*, *lane 3*). The excess IRAK-4 eluted at a position consistent with a monomer. To confirm the mass of the hMyD88-IRAK-4 complex, we also carried out sedimentation velocity AUC. The *c(S)* distribution shows a single predominant peak at 6.33 S, which from a *c(M)* analysis corresponds to a molecular mass of 173 kDa (Fig. 2*B*).

The molecular mass observed in the AUC experiments could be accounted for by several hMyD88-IRAK-4 stoichiometries, so to obtain a more accurate mass, the IRAK-4-hMyD88 complex was analyzed by nano-electrospray ionization mass spectroscopy under conditions that preserve the non-covalent interactions of the complex. The exceptional mass accuracy and resolving power of mass spectrometry can be used to determine unambiguous stoichiometries; this technique can be especially useful for complexes with heterogeneous or dynamic compositions (25). The mass spectra of the hMyD88-IRAK-4 complex (Fig. 2*C*) reveal a heterogeneous composition, with two overlapping charge series, corresponding to a major component with a mass of 165,800 ± 34 Da and a second of mass 182,372 ± 6 Da; these masses are consistent with MyD88-IRAK-4 stoichiometries of 7:4 (theoretical mass 165,725 Da)

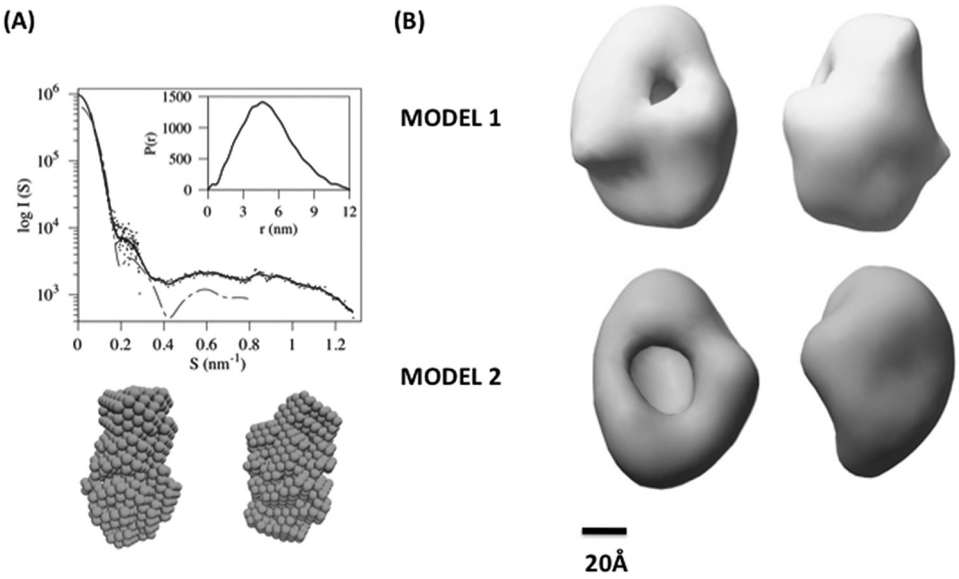

FIGURE 3. **Structural analysis of the hMyd88-IRAK-4 complexes.** *A*, x-ray scattering profiles of the hMyD88-IRAK-4 death domain oligomer. Also shown is the theoretical scattering profile for the PIDDosome core complex (*gray line*), calculated from the crystal structure of the PIDD-RAIDD death domain complex (PDB code 2of5). The distance distribution functions are shown as *insets* from which maximum particle dimensions 12.3 nm are obtained. Two orthogonal orientations of the *ab initio* models of the hMyD88-IRAK-4 complex are also shown. *B*, three-dimensional image reconstructions of the MyD88 complexes. Two views of the model are shown rotated through 90° (see also supplemental Fig. 2).

and 8:4 (theoretical mass 182,280 Da), respectively. Several weaker peaks are also evident but are not sufficiently resolved to make confident assignments, suggesting that further minor stoichiometries may be present. The 7:4 and 8:4 assignments are confirmed by the observation of "stripped complex" ion series generated by gas phase dissociation events at higher activation energies, including tandem mass spectrometry experiments where specific parent ions are isolated prior to activation. These experiments show stoichiometries of 6:4, 7:3, and 8:3 after ejection of single subunits (supplemental Fig. S1) and very weak ion series of 6:3 and 7:2 stoichiometry, suggesting that a 7:3 parent complex may also be present. Both the IRAK-4 and the MyD88 subunits are able to be ejected during gas phase dissociation; this may suggest that both kinds of subunit are present in surface-accessible sites in the complex, although the factors governing which subunit is ejected from a heteromeric complex remain a matter of debate (26).

Previous work has shown that the MyD88 ID (Fig. 1*A*) is essential for binding of IRAK-4 into post-receptor complexes and for activation of downstream signaling (6). To test whether the ID was also required for assembly of the Myddosome, we prepared a MyD88 protein truncated by 10 amino acids at the C terminus. This protein was unable to form the Myddosome assemblies, showing that an intact intermediate domain of MyD88 is essential for the formation of this complex as well as for signaling *in vivo* (result not shown).

Structural Analysis Reveals a Closed Complex Analogous to That of the PIDDosome—We have used small angle x-ray scattering (SAXS) and electron microscopy to study the structure of the hMyD88-IRAK-4 death domain assembly. Fig. 3*A* shows the x-ray scattering profiles for the complex together with *ab initio* models generated from SAXS data and the theoretical scattering profile of the PIDD-RAIDD death domain complex. The distance distribution function, *P(r)*, provides an estimate of the maximum linear dimension, d_{max}, and the value for the complex is 120 Å. The calculated scattering profile for the PIDD-RAIDD DD complex (Protein Data Bank (PDB) code 2OF5) and that measured for the hMyD88-IRAK-4 DD complex are qualitatively similar despite the larger size of hMyD88-IRAK-4 DD complex, suggesting that both complexes share a common architecture.

Samples of the complexes were also negatively stained and analyzed using electron microscopy. This reveals two major classes of particle, and the structure of these at 28 Å was determined using image reconstruction (Fig. 3*B*, *MODEL 1* and *MODEL 2*; , see also supplemental Fig. S2). The two structures are clearly related and have dimensions of ~100 × 75 × 60 Å. Both have a cavity in the top surface but are enclosed at the bottom, although it is noticeable that the cavity in Model 1 is smaller than that of the second. The first structure also appears to be more asymmetrical than the second. Interestingly, the PIDDosome has two rings of five death domains, and the subunits are packed closely together with no cavity being observed and a maximum dimension of about 75 Å. This indicates that the top surface of the Myddosome complex may be composed of more than five subunits. Taken together, the SAXS and electron microscopy data suggest a two-layered arrangement for the Myddosome. Model 1 may correspond to the 7:4, and the more symmetrical Model 2 may correspond to the 8:4 stoichiometries defined by the mass spectrometry studies.

Receptor Clustering Is Required to Initiate Signal Transduction by the Toll-like Receptor 4—The formation of the Myddosome *in vitro* strongly suggests that the TLR signaling process requires an oligomeric signaling platform similar to the death-induced signaling complex (DISC) formed by the Fas and FADD death domains during apoptotic signaling through the tumor necrosis factor pathway (27). In light of this prediction, we asked whether antibody-induced clustering of TLR4 was sufficient to activate signaling. To do this, we used the anti-TLR4 monoclonal antibody HTA125, a weak antagonist of TLR4 in solution (28). To induce receptor clustering, we immobilized HTA125 on the surface of high protein binding culture dishes at different concentrations and then plated out HEK293 cells stably transfected with TLR4. We then assayed for activation of the TLR4 pathway by measuring the concentration of the cytokine IL-8 in the culture supernatant. As shown in Fig. 4*A*, IL-8 was not produced when cells were plated on a low density of HTA125, but there was a rapid

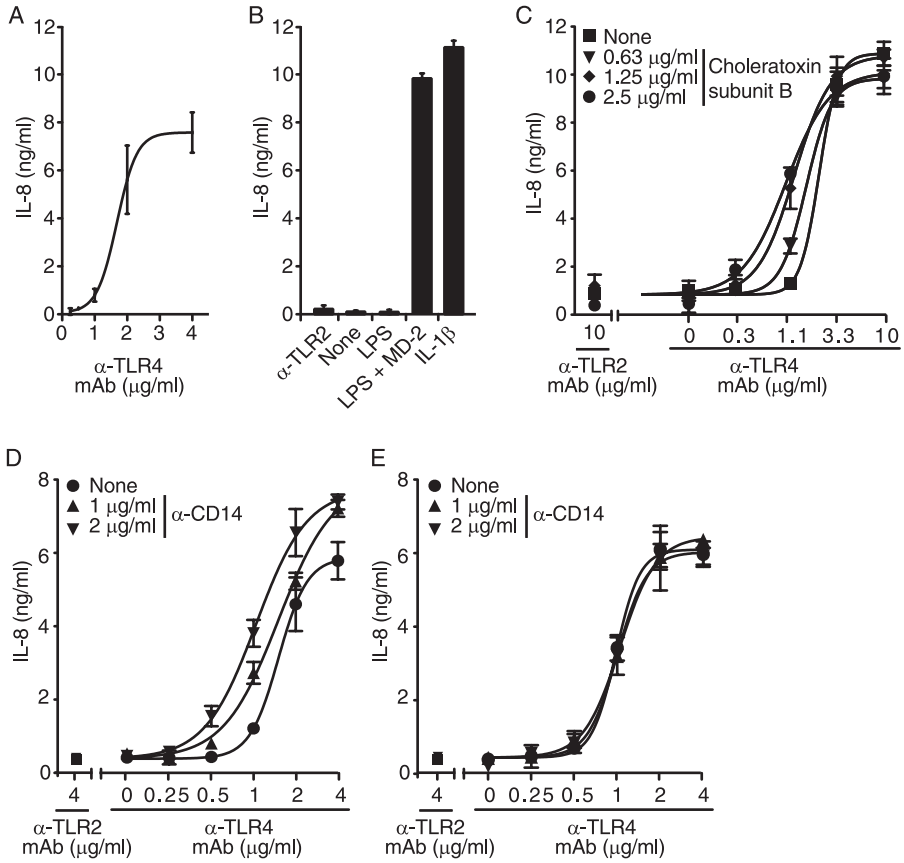

FIGURE 4. **Density-dependent activation of TLR4 by the antagonistic antibody HTA125.** HEK293-TLR4-YFP cells were cultured on polystyrene plastic previously coated with increasing concentrations of anti-TLR4 monoclonal antibody (*mAb*) (HTA125) (*A*) or control anti-TLR2 mAB (TL2.1), or cells were treated with LPS (100 ng/ml), LPS (100 ng/ml) with MD-2 (conditioned supernatants), or IL-1β (100 ng/ml) (*B*). IL-8 secretion into supernatants was assessed by ELISA. *C*, HTA125 or TL2.1 was immobilized alone or together with increasing concentration of cholera toxin subunit B. HEK293-TLR4-YFP cells were subsequently plated, and IL-8 secretion was measured in supernatants by ELISA. HEK293-TLR4-YFP (*D*) or HEK293-TLR4-YFP-CD14 cells (*E*) were cultured on polystyrene previously coated with HTA125 alone or with increasing concentrations of anti-CD14 (26ic) monoclonal antibody. IL-8 was measured in supernatants by ELISA. Shown are means and S.D. (*error bars*) of triplicates of representative experiments of three (*A*, *B*, and *C*) or two (*D* and *E*) repeats. *B*, cholera toxin subunit B enhances the ability of HTA125 to activate the TLR4 pathway. *C*, HTA125 activates TLR4 independently of lipopolysaccharide. A control antibody against TLR2 is ineffective in this assay. *Open squares*, no treatment; *triangles*, 0.5 ng ml^{-1} LPS; *closed squares*, 5 ng ml^{-1}; *diamonds*, 50 ng ml^{-1}.

activation of the TLR4 pathway at concentrations above 1.1 μg ml^{-1} of antibody. In fact, IL-8 production is activated from baseline levels to maximum by a 3-fold increase in antibody density, a dose response that is characteristic of a process displaying positive cooperativity (29). This antibody-induced receptor clustering led to almost maximal cell activation when compared with maximal TLR4 activation by LPS and MD2 or IL-1β (Fig. 4*B*).

TLR4 signaling requires the lipid raft microdomain-associated adaptor molecules Mal and TRIF-related adaptor molecule (TRAM) for the initiation of signaling via MyD88 or TRIF. We next tested whether forced co-recruitment of lipid raft microdomains into the antibody-induced TLR4 receptor clusters could enhance the signaling efficiency. Cholera toxin subunit B binds and cross-links the minor membrane lipid GM2 ganglioside in lipid raft microdomains. We therefore immobilized purified cholera toxin subunit B at increasing concentrations together with the TLR4 antibody HTA125 (Fig. 4*C*). Indeed, recruitment of lipid raft components into the TLR4 receptor cluster by cholera toxin subunit B dose-dependently enhanced the ability of HTA125 to induce cytokine production (Fig. 4*C*). These data indicate that signals that increase the density of adaptor molecules at the site of TLR4 clustering promote a cooperative effect in MyD88 signaling. LPS is known to bind to the glycosylphosphatidylinositol-linked microdomain-associated molecule CD14 (30), and CD14 expression can dramatically enhance the ability of cells to respond to CD14. We therefore examined whether co-clustering CD14 together with TLR4 can also increase the efficiency of TLR4 activation. Similar to what we observed with co-clustering of rafts by use of cholera toxin subunit B, CD14 clustering also led to a dose-responsive increase of TLR4 clustering-induced activation in cells that expressed CD14 (Fig. 4*D*) but not in cells that lacked CD14 expression (Fig. 4*E*). Together, these data indicate that clustering of TLR4 even in the absence of MD2 and LPS is sufficient to induce TLR4 activation and that the local concentration of raft-associated molecules can dramatically increase the efficiency to TLR4-induced signaling.

DISCUSSION

In this study, we describe the complex behavior of the MyD88 death domain, which reversibly self-associates to form higher order oligomers. In a previous study, Burns *et al.* (4) showed that a mutation, F56N, abolishes the ability of MyD88 DDs to interact with itself in a yeast two-hybrid assay. Phe-56 is equivalent to Tyr-814 in the PIDD death domain, a residue that lies in the type 1 interface formed by PIDD-PIDD and PIDD-RAIDD contacts observed in the PIDDosome. Thus one mode of hMyD88 self-association may be mediated by a type 1 interface. Interestingly, a chemical cross-linker is only able to generate covalent dimers of hMyD88 DD but not the higher order oligomers observed in solution. This finding suggests that only one type of binding interface can bring two lysine side chains close enough together to react with the cross-linker. In that regard, the death domain of MyD88 has only a single lysine residue in the C terminus of the death domain, although there are several present in the ID. Together, these findings suggest that the DD of hMyD88 can self-associate by type 1 DD-DD interactions and DD-ID or ID-ID interactions.

Unlike hMyD88 alone, the death domains of hMyD88 and IRAK-4 associate to produce a large oligomeric assembly, a property similar to that displayed by the PIDD and RAIDD death domains that form the PIDDosome. The low resolution structural

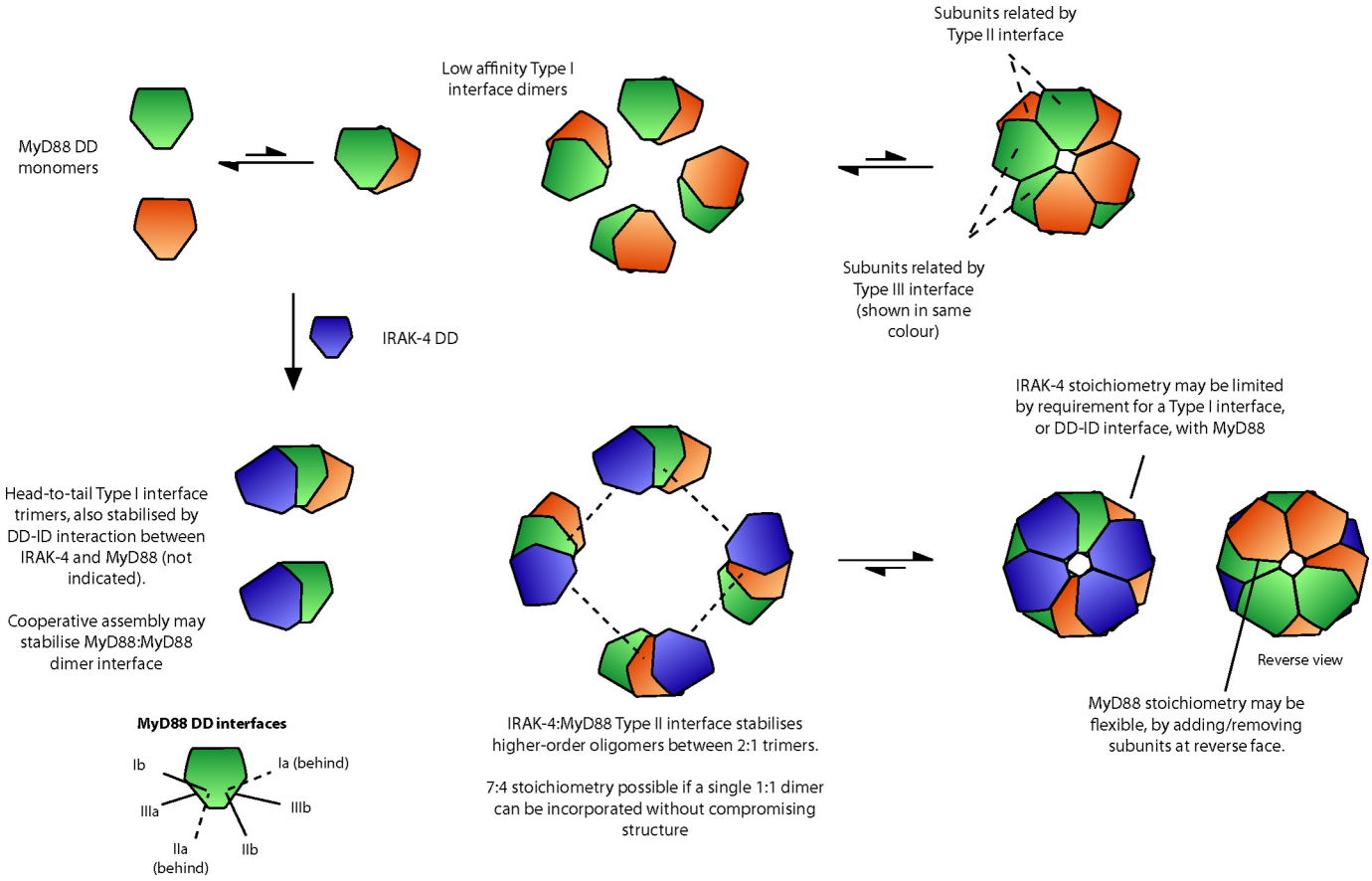

FIGURE 5. **Potential assembly pathway for the Myddosome.**

data we have obtained do not allow the arrangement of the subunits in the complex to be determined. However, we propose that seven or eight MyD88 subunits create a ring that is further stabilized by the binding of four IRAK-4 molecules into a second layer. A possible arrangement of subunits in an 8:4 complex is shown in Fig. 5. The model predicts that MyD88 dimerizes via a type 1 interface and that an IRAK-4 subunit can then bind to form a trimer with a head-to-tail arrangement of type 1 interfaces. Four heterotrimers would then assemble into a stable complex with IRAK-4-MyD88 type 2 stabilizing the higher order oligomer. This model can account for the observed 7:4 stoichiometry because a MyD88-IRAK-4 heterodimer would be able to assemble with three heterotrimers with little loss of stability. By contrast, the IRAK-4 stoichiometry would be fixed by the requirement for a type 1 or DD-ID interface with MyD88. This arrangement is consistent with that seen in the PIDDosome in which type 2 interactions stabilize the interface between the bottom layer of PIDD subunits and the second layer of RAIDDs. The assembly process may display positive cooperativity similar to that recently demonstrated in the binding of the *Drosophila* IRAK-4 homologue, Pelle, with a dimer of the signaling adaptors Tube and dMyD88 (see below) (31). The assembly process may also create a scaffold for the recruitment of IRAK-1, which unlike IRAK-4 is recruited into MyD88 complexes by DD-DD interactions and does not require the ID. It should be noted that alternative arrangements for the subunits of the Myddosome are possible.

Our finding that two key signal transducers in the IL-1 and TLR signaling pathways assemble into a defined oligomeric complex has implications for the overall mechanism of signal transduction by these receptors. A possible scenario is that in the unstimulated state, full-length hMyD88 is inhibited from forming higher order complexes. Upon receptor activation, two MyD88 TIR domains bind to the receptor TIR homodimer (5) (or in the case of TLR4, a heterotetramer with the Mal adaptor), and this induces a conformational change enabling the hMyD88 death domain to assemble with IRAK-4 into a Myddosome. This model is consistent with a recent study by Ohnishi *et al.* (32), which describes a structure of the MyD88 TIR domain. This work shows that TIR is a monomer in solution, and thus it is likely that the death domain alone has the ability to oligomerize. The study also identifies residues critical for binding to the Mal adaptor, confirming that the adaptor TIR domain initiates formation of the activated receptor scaffold. Incorporation of IRAK-4 death domain into the Myddosome may activate the kinase by unblocking the active site.

The ability to form both 7:4 and 8:4 stoichiometries suggests a mechanism by which clusters of activated receptors might form. Thus the 7:4 Myddosome would link together three pairs of activated receptors and the seventh MyD88 protomer would be able to cross-link with another 8:4 assembly. This arrangement would allow clusters of alternating 7:4 and 8:4 Myddosomes to form. This behavior is similar to that observed in the death signaling pathway mediated by the Fas receptor. Activation of the receptor by the Fas ligand results in the formation of the DISC, a highly oligomeric signaling platform formed from the Fas and FADD death domains. A recent report shows

that the initial event in DISC formation is the self-association of Fas and that this requires a switch in which helix 5 of the death domain adopts an extended conformation (27). This switch is initiated in response to ligand and is enhanced by the accumulation of Fas receptor molecules into lipid rafts. Furthermore, previous studies demonstrated that activation causes TLR2 and TLR4 to accumulate in lipid rafts (33). Clustering of the TLRs leads to a substantial decrease in the diffusion coefficient of TLR4, presumably due the formation of very large oligomeric assemblies of the type we describe here (34).

It is also likely that different activated TLRs, for example TLR4 and TLR1/2, could be recruited into the same assembly and may explain the synergistic effect of different TLR activators. Thus low concentrations of TLR4 and TLR2 agonists that do not activate signaling elicit a strong response when applied together (35). This synergy could be explained if activated TLR4 and TLR2 dimers can assemble into the same Myddosome complex and if, as proposed, Myddosome assembly displays positive cooperativity.

It is informative to compare the properties of the post-receptor DD containing molecules in TLR signaling with their homologues from the *Drosophila* Toll pathway. In the Toll pathway, the activated receptor recruits a heterotrimer comprising the death domains of dMyD88, the homologue of hMyD88, a bifunctional DD adaptor Tube, and the kinase Pelle, which is the homologue of IRAK-4 (31, 36). The DD of Pelle and dMyD88, like those of IRAK-4 and hMyD88, are monomeric. Nevertheless, recruitment of two dMyD88 molecules to an activated receptor may promote the formation of a type 1 dMyD88 homodimer interface with tube binding to the symmetrically related type 1 site or by a type 2 interaction. In this regard, many of the residues involved in type 1 interfaces are conserved between *Drosophila* and hMyD88. However, despite this conservation, Pelle and dMyD88 are unable to assemble into oligomeric complexes, and furthermore, no interaction can be detected between them. An intriguing difference between the insect and vertebrate pathways is that the latter do not have a homologue of Tube, which presumably has been lost during evolution. Potentially, a new mode of interaction between IRAK-4 and hMyD88 arose and enabled the formation of the higher order oligomeric assemblies we describe here. Tube then became functionally redundant and was lost.

The Myddosome may account for the more complex patterns of regulation observed in the vertebrate TLR pathways. For example, such a scaffold could support the recruitment of further regulatory molecules such as IRAK-2 (37), IRAK-M (38), and Tollip (39) and other signal transducers such as IRF-7 (40) and FADD (41) that branch from the signaling pathway at the level of hMyD88.

REFERENCES

1. Akira, S., Uematsu, S., and Takeuchi, O. (2006) *Cell* **124,** 783–801
2. Gay, N. J., and Gangloff, M. (2007) *Annu. Rev. Biochem.* **76,** 141–165
3. O'Neill, L. A., and Bowie, A. G. (2007) *Nat. Rev. Immunol.* **7,** 353–364
4. Burns, K., Martinon, F., Esslinger, C., Pahl, H., Schneider, P., Bodmer, J. L., Di Marco, F., French, L., and Tschopp, J. (1998) *J. Biol. Chem.* **273,** 12203–12209
5. Núñez Miguel, R., Wong, J., Westoll, J. F., Brooks, H. J., O'Neill, L. A., Gay, N. J., Bryant, C. E., and Monie, T. P. (2007) *PLoS ONE* **2,** e788
6. Burns, K., Janssens, S., Brissoni, B., Olivos, N., Beyaert, R., and Tschopp, J. (2003) *J. Exp. Med.* **197,** 263–268
7. Brikos, C., Wait, R., Begum, S., O'Neill, L. A., and Saklatvala, J. (2007) *Mol. Cell Proteom.* **6,** 1551–1559
8. Neumann, D., Kollewe, C., Resch, K., and Martin, M. U. (2007) *Biochem. Biophys. Res. Commun.* **354,** 1089–1094
9. Kollewe, C., Mackensen, A. C., Neumann, D., Knop, J., Cao, P., Li, S., Wesche, H., and Martin, M. U. (2004) *J. Biol. Chem.* **279,** 5227–5236
10. Weber, C. H., and Vincenz, C. (2001) *Trends Biochem. Sci.* **26,** 475–481
11. Xiao, T., Towb, P., Wasserman, S. A., and Sprang, S. R. (1999) *Cell* **99,** 545–555
12. Qin, H., Srinivasula, S. M., Wu, G., Fernandes-Alnemri, T., Alnemri, E. S., and Shi, Y. (1999) *Nature* **399,** 549–557
13. Park, H. H., Logette, E., Raunser, S., Cuenin, S., Walz, T., Tschopp, J., and Wu, H. (2007) *Cell* **128,** 533–546
14. Latz, E., Visintin, A., Lien, E., Fitzgerald, K. A., Monks, B. G., Kurt-Jones, E. A., Golenbock, D. T., and Espevik, T. (2002) *J. Biol. Chem.* **277,** 47834–47843
15. Davies, O. R., and Pellegrini, L. (2007) *Nat. Struct. Mol. Biol.* **14,** 475–483
16. Schuck, P. (2000) *Biophys. J.* **78,** 1606–1619
17. Svergun, D. I. (1992) *J. Appl. Crystallog.* **25,** 495–503
18. Svergun, D. I., Petoukhov, M. V., and Koch, M. H. (2001) *Biophys. J.* **80,** 2946–2953
19. Volkov, V., and Svergun, D. (2003) *J. Appl. Crystallog.* **36,** 860–864
20. Kozin, M., and Svergun, D. (2001) *J. Appl. Crystallog.* **34,** 33–41
21. Hernández, H., and Robinson, C. V. (2007) *Nat. Protoc.* **2,** 715–726
22. Ludtke, S. J., Baldwin, P. R., and Chiu, W. (1999) *J. Struct. Biol.* **128,** 82–97
23. Murali, A., Li, X., Ranjith-Kumar, C. T., Bhardwaj, K., Holzenburg, A., Li, P., and Kao, C. C. (2008) *J. Biol. Chem.* **283,** 15825–15833
24. Pettersen, E. F., Goddard, T. D., Huang, C. C., Couch, G. S., Greenblatt, D. M., Meng, E. C., and Ferrin, T. E. (2004) *J. Comput. Chem.* **25,** 1605–1612
25. Sharon, M., and Robinson, C. V. (2007) *Annu. Rev. Biochem.* **76,** 167–193
26. Benesch, J. L. (2009) *J. Am. Soc. Mass Spectrom.* **20,** 341–348
27. Scott, F. L., Stec, B., Pop, C., Dobaczewska, M. K., Lee, J. J., Monosov, E., Robinson, H., Salvesen, G. S., Schwarzenbacher, R., and Riedl, S. J. (2009) *Nature* **457,** 1019–1022
28. Shimazu, R., Akashi, S., Ogata, H., Nagai, Y., Fukudome, K., Miyake, K., and Kimoto, M. (1999) *J. Exp. Med.* **189,** 1777–1782
29. Koshland, D. E., Jr. (1996) *Curr. Opin. Struct. Biol.* **6,** 757–761
30. Wright, S. D., Ramos, R. A., Tobias, P. S., Ulevitch, R. J., and Mathison, J. C. (1990) *Science* **249,** 1431–1433
31. Moncrieffe, M. C., Grossmann, J. G., and Gay, N. J. (2008) *J. Biol. Chem.* **283,** 33447–33454
32. Ohnishi, H., Tochio, H., Kato, Z., Orii, K. E., Li, A., Kimura, T., Hiroaki, H., Kondo, N., and Shirakawa, M. (2009) *Proc. Natl. Acad. Sci. U.S.A.* **106,** 10260–10265
33. Triantafilou, M., Morath, S., Mackie, A., Hartung, T., and Triantafilou, K. (2004) *J. Cell Sci.* **117,** 4007–4014
34. Triantafilou, M., Brandenburg, K., Kusumoto, S., Fukase, K., Mackie, A., Seydel, U., and Triantafilou, K. (2004) *Biochem. J.* **381,** 527–536
35. Beutler, E., Gelbart, T., and West, C. (2001) *Blood Cells Mol. Dis.* **27,** 728–730
36. Sun, H., Towb, P., Chiem, D. N., Foster, B. A., and Wasserman, S. A. (2004) *EMBO J.* **23,** 100–110
37. Keating, S. E., Maloney, G. M., Moran, E. M., and Bowie, A. G. (2007) *J. Biol. Chem.* **282,** 33435–33443
38. Kobayashi, K., Hernandez, L. D., Galán, J. E., Janeway, C. A., Jr., Medzhitov, R., and Flavell, R. A. (2002) *Cell* **110,** 191–202
39. Zhang, G., and Ghosh, S. (2002) *J. Biol. Chem.* **277,** 7059–7065
40. Honda, K., Yanai, H., Negishi, H., Asagiri, M., Sato, M., Mizutani, T., Shimada, N., Ohba, Y., Takaoka, A., Yoshida, N., and Taniguchi, T. (2005) *Nature* **434,** 772–777
41. Zhande, R., Dauphinee, S. M., Thomas, J. A., Yamamoto, M., Akira, S., and Karsan, A. (2007) *Mol. Cell. Biol.* **27,** 7394–7404